Linear and Non-Linear Transonic Flow Behaviour of the Goland$^+$ wing

Gareth A. Vio[1], Grigorios Dimitriadis[2], Jonathan E. Cooper[2,3] and Kenneth J. Badcock[1]

[1]Department of Engineering, The University of Liverpool
Liverpool L69 3GH, UK

[2]School of Mechanical, Aerospace and Civil Engineering
The University of Manchester, PO Box 88, Manchester M60 1QD, UK

[3]e-mail: jecooper@manchester.ac.uk

Keywords: CFD/CSD, Transonic Aerodynamics, Aeroelasticity, Bifurcation, ROM

Abstract. This paper is part of a study investigating the prediction of the aeroelastic behavior of aircraft subjected to transonic aerodynamic forces. The main objective of the work is the creation of Reduced Order Models from coupled Computational Fluid Dynamic and Finite Element calculations. The novelty of the approach lies in the identification of different types of Reduced Order Model in different flight regimes. Linear modal models are used in the Mach range range where the full CFD/CSD system is linear and nonlinear modal models in the transonic flight regime where the CFD/CSD system undergoes Limit Cycle Oscillations. Static solutions of the CFD/CSD system are used in order to determine the extent of the nonlinear Mach number range. The model treated in this work is a three-dimensional wing in a transonic flowfield.

1 INTRODUCTION

The influence of nonlinearities on modern aircraft and the requirement for more accurate tools for the prediction of their effects are becoming increasingly important. These nonlinearities occur due to structural (freeplay, hysteresis, cubic stiffness), aerodynamic (transonic effects) or control system (control laws, control surface deflection and rate limits) phenomena. Of particular interest is the prediction of Limit Cycle Oscillations (LCO) which cannot be performed if a linear structural and/or aerodynamic model is used for analysis purposes.

Although not destructive in the same sense as flutter, LCO can lead to fatigue and pilot control problems. A further difficulty is the case of an unpredicted LCO occurring during the flight flutter test programme, as the question then arises as to whether the vibration is flutter or LCO [1]. A significant amount of expensive testing is currently required to resolve this type of problem.

There has been much work determining the effects of structural non-linearities on low order simulated aeroelastic systems [2, 3] and also experimental studies [4]. Recent studies have investigated the use of mathematical techniques to predict the amplitude of the LCO without recourse to numerical integration e.g. using Normal Form [5], Higher Order Harmonic Balance [6, 7] and other methods [8, 9].

A substantial amount of research has been directed recently towards modelling the effect of nonlinear aerodynamics on aeroelastic systems in the transonic regime. Such coupled CFD/CSD calculations are expensive and therefore there is a need to produce Reduced Order Models (ROM) [10] of aeroelastic systems that can be used to determine and characterise the dynamic behaviour and stability boundaries. The CFD/CSD can then be directed towards the most critical flight regions of interest.

One means of obtaining Reduced Order Models is to curve-fit the data obtained from coupled CFD/CSD models. Recent work in this area has included the use of higher order spectral methods [11] and Volterra Series [12, 13, 14]. Another means of obtaining ROMs is directly from the CFD/CSD system using Proper Orthogonal Decomposition [15, 16]. In fact, ROM creation is currently a very active area of research in Aeroelasticity.

One aspect of the analysis of aeroelastic systems containing structural non-linearities is that these non-linearities are always present and are related to a certain point of the structure. However, aerodynamic non-linearities only occur during transonic flight speeds and are not related to specific parts of the lifting surfaces as the shocks move about on the structure. Vio et al [17] showed that aeroelastic systems are intermittently nonlinear, being completely linear in most of the flight envelope and nonlinear in a narrow range of Mach numbers.

In this paper, the dependence of nonlinear aerodynamics on flight condition is exploited in order to derive two different types of Reduced Order Models. A simple linear modal model is used at flight conditions where the full aeroelastic system is linear and a nonlinear modal model is used in order to characterize the LCO behaviour in the nonlinear Mach number range. The nonlinear dynamics of the Goland Wing CFD/CSD model at different flight speeds are analysed in order to determine their complexity. Static aerodynamic solutions of the Goland Wing are used to predict the Mach range in which nonlinear phenomena are important.

2 AERODYNAMIC AND STRUCTURAL MODELLING

2.1 Aerodynamics

The three-dimensional Euler equations can be written in conservative form and Cartesian coordinates as

$$\frac{\partial \boldsymbol{w}_f}{\partial t} + \frac{\partial \boldsymbol{F}^i}{\partial x} + \frac{\partial \boldsymbol{G}^i}{\partial y} + \frac{\partial \boldsymbol{H}^i}{\partial z} = 0 \tag{1}$$

where $\boldsymbol{w}_f = (\rho; \rho u; \rho v; \rho w; \rho E)^T$ denotes the vector of conserved variables. The flux vectors $\boldsymbol{F}^i$, $\boldsymbol{G}^i$ and $\boldsymbol{H}^i$ are

$$\boldsymbol{F}^i = \begin{pmatrix} \rho U^* \\ \rho u U^* + p \\ \rho v U^* \\ \rho w U^* \\ U^*(\rho E + p) + \dot{x} \end{pmatrix}$$

$$\boldsymbol{G}^i = \begin{pmatrix} \rho V^* \\ \rho u V^* \\ \rho v V^* + p \\ \rho w V^* \\ V^*(\rho E + p) + \dot{y} \end{pmatrix} \quad \boldsymbol{H}^i = \begin{pmatrix} \rho W^* \\ \rho u W^* \\ \rho v W^* + p \\ \rho w W^* + p \\ W^*(\rho E + p) + \dot{z} \end{pmatrix} \tag{2}$$

where ρ, u, v, w, p and E denote the density, the three Cartesian components of the velocity, the pressure and the specific total energy respectively, and U^*, V^*, W^* the three Cartesian components of the velocity relative to the moving coordinate system which has local velocity components $\dot{x}$, $\dot{y}$ and $\dot{z}$ i.e.

$$U^* = u - \dot{x} \quad (3)$$
$$V^* = v - \dot{y} \quad (4)$$
$$W^* = w - \dot{z} \quad (5)$$

The flow solution in the current work is obtained using the PMB (parallel multi-block) code, and a summary of some applications examined using the code can be found in reference [18].

A fully implicit steady solution of the Euler equations is obtained by advancing the solution forward in time by solving the discrete nonlinear system of equations

$$\frac{\boldsymbol{w}_f^{n+1} - \boldsymbol{w}_f^n}{\Delta t} = \boldsymbol{R}_f\left(\boldsymbol{w}_f^{n+1}\right) \quad (6)$$

The term on the right hand side, called the residual, is the discretization of the convective terms, given here by Osher's approximate Riemann solver [19], MUSCL interpolation [20] and Van Albada's limiter. The sign of the definition of the residual is opposite to convention in CFD but this is to provide a set of ordinary differential equations which follows the convention of dynamical systems theory, as will be discussed in the next section. Equation 6 is a nonlinear system of algebraic equations. These are solved by an implicit method [21], the main features of which are an approximate linearization to reduce the size and condition number of the linear system, and the use of a preconditioned Krylov subspace method to calculate the updates. The steady state solver is applied to unsteady problems within a pseudo time stepping iteration [22].

2.2 Structural Dynamics, Inter-grid Transformation and Mesh Movement

The wing deflections δx_s are defined at a set of points x_s by

$$\delta \boldsymbol{x}_s = \sum \alpha_i \phi_i \quad (7)$$

where ϕ_i are the mode shapes calculated from a full finite element model of the structure and α_i are the generalised coordinates. By projecting the finite element equations onto the mode shapes, the scalar equations

$$\frac{d^2\alpha_i}{dt^2} + \omega_i^2 \alpha_i = \mu \phi_i^T \boldsymbol{f}_s \quad (8)$$

are obtained where $\boldsymbol{f}_s$ is the vector of aerodynamic forces at the structural grid points and μ is a coefficient related to the fluid free stream dynamic pressure which redimensionalises the aerodynamic forces. These equations are rewritten as a system in the form

$$\frac{d\boldsymbol{w}_s}{dt} = \boldsymbol{R}_s \quad (9)$$

with $\boldsymbol{w}_s = (\ldots, \alpha_i, \dot{\alpha}_i, \ldots)^T$ and $\boldsymbol{R}_s = (\ldots, \dot{\alpha}_i, \mu\phi_i^T \boldsymbol{f}_s - \omega^2 \alpha_i, \ldots)^T$

The aerodynamic forces are calculated at cell centres on the aerodynamic surface grid. The problem of communicating these forces to the structural grid is complicated in the common situation where these grids not only do not match, but also are not defined on the same surface.

This problem, and the influence it can have on the aeroelastic response, was considered in [23], where a method was developed called the constant volume tetrahedron (CVT) transformation. This method uses a combination of projection of fluid points onto the structural grid, transformation of the projected point and recovery of the out-of-plane component to obtain a cheap, but effective, relation between deformations on the structural grid and those on the fluid grid.

Denoting the fluid grid locations and aerodynamic forces as x_a and $\boldsymbol{f}_a$, then

$$\delta \boldsymbol{x}_a = \boldsymbol{S}(\boldsymbol{x}_a, \boldsymbol{x}_s, \delta \boldsymbol{x}_s) \tag{10}$$

where $\boldsymbol{S}$ denotes the relationship defined by CVT. In practice this equation is linearised to give

$$\delta \boldsymbol{x}_a = S(\boldsymbol{x}_a, \boldsymbol{x}_s)\delta \boldsymbol{x}_s \tag{11}$$

and then by the principle of virtual work $\boldsymbol{f}_s = S^T \boldsymbol{f}_a$

The grid speeds on the wing surface are also needed and these are approximated directly from the linearised transformation as

$$\delta \dot{\boldsymbol{x}}_a = S(\boldsymbol{x}_a, \boldsymbol{x}_s)\delta \dot{\boldsymbol{x}}_s \tag{12}$$

where the structural grid speeds are given by

$$\delta \dot{\boldsymbol{x}}_s = \sum \dot{\alpha}_i \phi_i \tag{13}$$

The geometries of interest deform during the motion. This means, unlike the rigid aerofoil problem, that the aerodynamic mesh must be deformed rather than rigidly translated and rotated. This is achieved using transfinite interpolation of displacements (TFI) as described in reference [24]. The grid speeds are also interpolated from known boundary speeds. In this way the grid locations depend on α_i and the speeds on $\dot{\alpha}_i$.

2.3 Time Domain Solver

For coupled CFD/CSD calculations the aerodynamic and structural solutions must be sequenced. For steady solutions, taking one step of the CFD solver followed by one step of the structural solver will result in the correct equilibrium. However, for time accurate calculations more care must be taken to avoid introducing additional errors. The exact formulation used to avoid this is discussed by Goura et al [25].

3 AEROELASTIC RESULTS

In this study the Goland wing aeroelastic model [26, 27] was used. It is a straight rectangular wing with a symmetric wing section. The finite element model is presented in figure 1. This was built using CQUAD4 and CROD elements. A tip store rigidly attached to the wing is also included. The tip store does not participate in the aerodynamics. Figure 2 depicts the mode shapes of the first four modes. Mode 1 is pure bending, mode 2 pure torsion and modes 3 and 4 are combinations of bending and torsion. The wind-off natural frequencies vary between 1.71 Hz and 11.49 Hz, as shown in teh figure captions of figure 2.

Two types of tests were performed: static and dynamic. The static tests concerned the solution of the steady flowfield for an immobile wing at different Mach numbers and angles of attack.

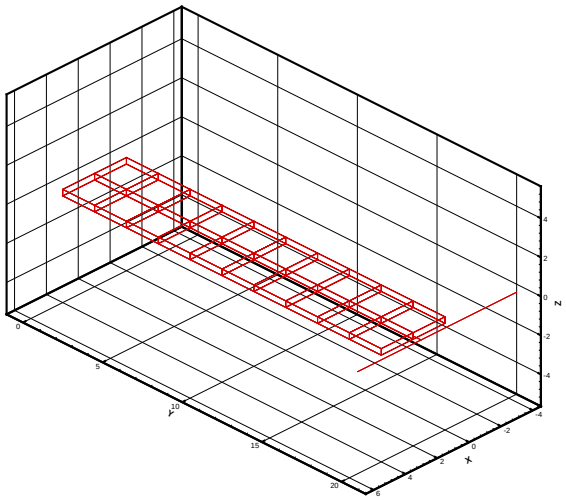

Figure 1: Goland wing finite element model

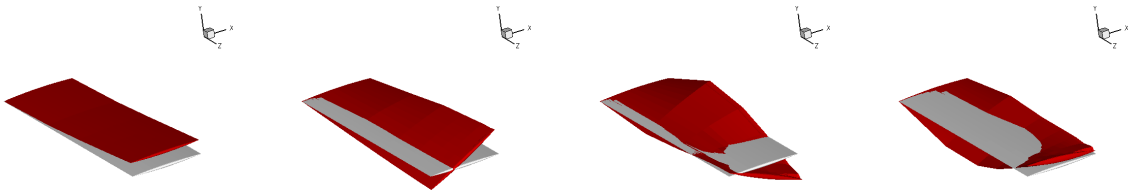

(a) Mode 1. ω_n=1.71 Hz (b) Mode 2. ω_n=3.05 Hz (c) Mode 3. ω_n=9.18 Hz (d) Mode 4. ω_n=11.39 Hz

Figure 2: Goland wing mode shapes

The dynamic results concerned the calculation of the impulse response of the Goland wing given initial velocity excitation at different Mach numbers.

3.1 Static Results

The object of the static results was to study the shape of the lift curve for the Goland wing at different Mach numbers and to identify Mach numbers at which shock waves can lie on the wing's surface. Static solutions were obtained for angles of attack of -10° to 10° at Mach numbers from 0.8 to 0.995. The resulting lift curves are plotted in the form of surface graphs in figure 3(a). The gaps in the data occurred because the solution failed to converge at those particular conditions.

Figure 3(a) shows that the shape of the lift curve is very nonlinear at Mach numbers from 0.8 to 0.95 and becomes approximately linear as the Mach number approaches 1. The maximum nonlinearity occurs at around $M = 0.85$.

Figure 3(b) shows just five of the lift curves, calculated at $M = 0.8, 0.85, 0.9, 0.945, 0.995$. The main nonlinear feature is a sudden change in slope, occurring at $\pm 5^\circ$ at $M = 0.8$ and which moves to lower angles of attack as the Mach number increases. This change in slope is most abrupt at $M = 0.85$. At $M = 0.995$ the lift curve appears completely linear. Figure 4 shows the values of the lift curve slope at different angles of attack and Mach numbers. It can be seen that there is a clear wedge-shaped area where there is a big discontinuity in lift curve slope,

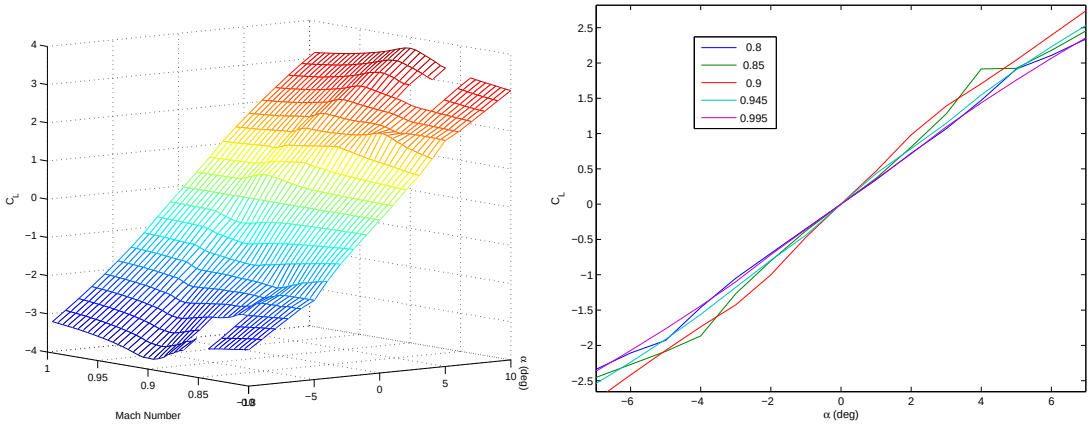

(a) Lift curve variation with Mach number (b) Lift curves at five Mach number

Figure 3: Lift curve variation with Mach number

starting at $\pm 5^\circ$ at low Mach numbers and reaching its apex at $M = 0.95$. Up to $M = 0.87$ the increase in slope as the angle of attack decreases is preceded by a big decrease in slope. This phenomenon disappears at $M = 0.88$. The biggest change in slope occurs at $M = 0.85$.

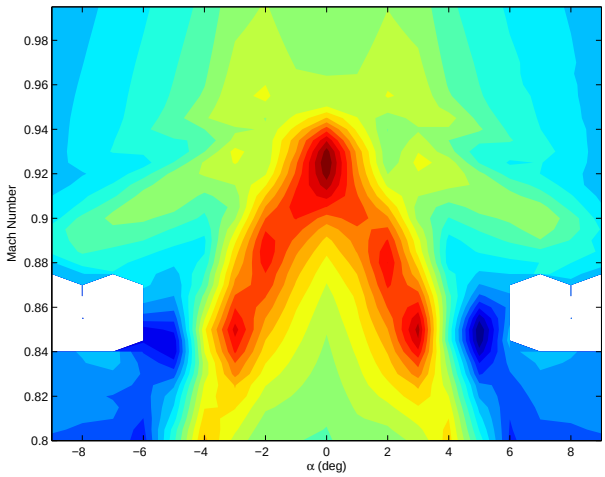

Figure 4: Lift curve slope at different angles of attack and Mach numbers

The reason for the occurrence of this slope change is, of course, the creation of a shock wave. At low Mach numbers a shock wave appears at high values of the angle attack, changing the behaviour of the flowfield and, consequently, the lift curve slope. At higher Mach numbers, the curvature of the airfoil is enough to accelerate the flow beyond Mach 1 locally so the shock wave appears at zero angle of attack.

Figure 5 plots the supersonic flow areas over the upper surface of the wing at 0° angle of attack and four different Mach numbers. The blue dots denote grid points at which the flow is calculated while the red circles denote areas where the flow is supersonic. It can be seen that the supersonic flow area appears as a very small area just behind the mid-chord point (which, for this airfoil, also happens to be the point of maximum thickness) and grows until at $M = 0.95$ it extends to the trailing edge. This means that the shock wave initially lies near the wing's centerline but at higher Mach numbers reaches the trailing edge.

In order to better understand the source of nonlinearity, the position of the shock wave was

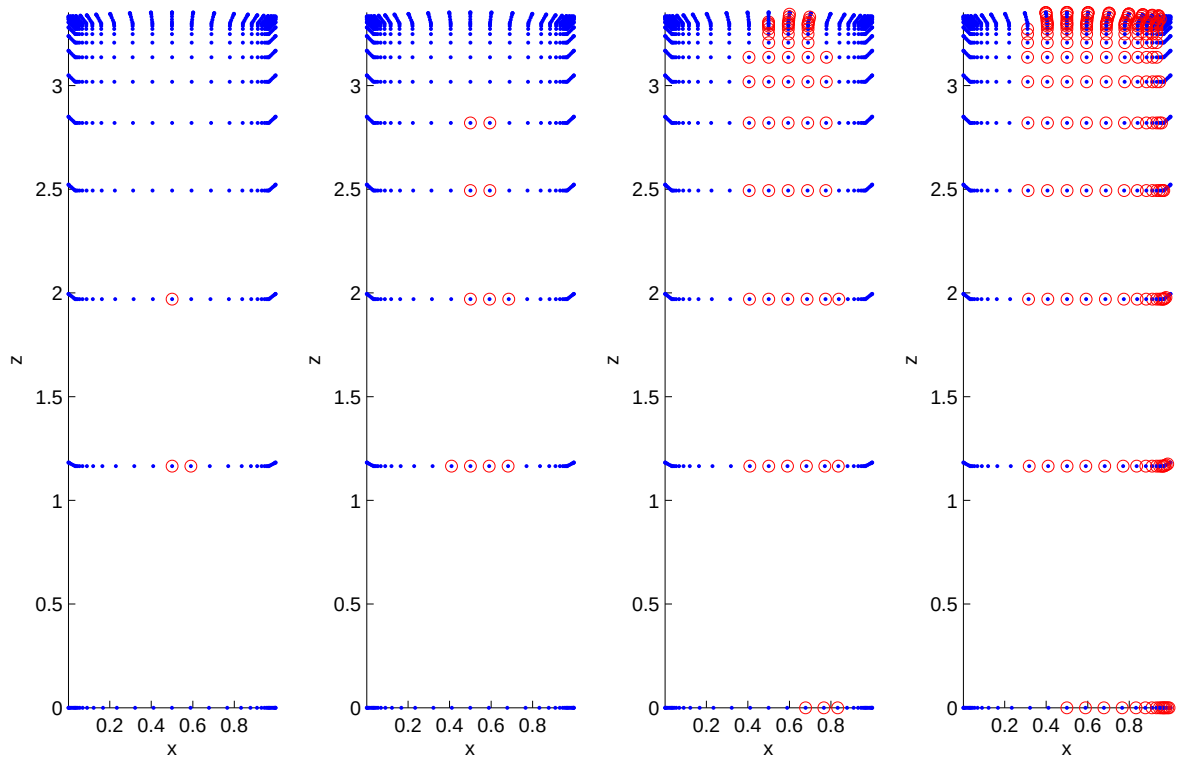

(a) $M = 0.885$ (b) $M = 0.9$ (c) $M = 0.92$ (d) $M = 0.95$

Figure 5: Areas of supersonic flow over Goland wing at 0° angle of attack

calculated for each free stream Mach number and angle of attack. Figure 6(a) shows the furthest aft position of the shock wave over the entire wing for each flight case. It can be seen that the shock wave can lie at the leading edge for low but non-zero angles of attack and Mach numbers. The figure suggests that a wing oscillating between -10° and 10° angle of attack in a quasi-steady fashion at Mach numbers from 0.8 to 0.85 will see a shock wave whose position will be oscillating between the leading edge and the trailing edge. At $M = 0.86$ the shock oscillates between $x/c = 0.6$ and the trailing edge.

The strongest nonlinearity occurs at $M = 0.85$ because it is the last Mach value at which the shock can lie at the leading edge and at the same time the shock strength is higher than at lower Mach numbers. Figure 6(b) shows the value of the maximum local Mach number for all free stream Mach numbers and angles of attack. There is a clear increasing tendency for all the local Mach numbers as the free stream Mach value is increased. The major conclusion to be drawn from the static results is that the nonlinearity depends on

- The distance that the shock wave can travel over the wing's surface
- The strength of the shock

The dynamic results to be presented in the next section were obtained for the case where the wing is fixed at zero angle of attack and is free to oscillate in bending and torsion. For this particular angle of attack figure 6(a) shows that shock waves can only exist on the wing surface between Mach numbers of 0.885 and 0.955. At $M \geq 0.955$, the shock wave lies on the trailing edge.

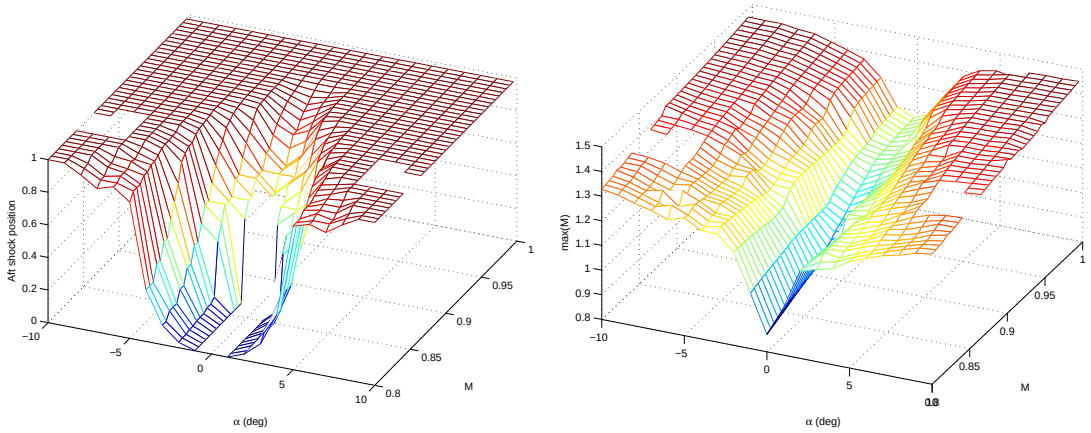

(a) Aft shock position (b) Maximum Mach number

Figure 6: Shock position and maximum local Mach number at various free stream Mach numbers and angles of attack

3.2 Dynamic Results

Full dynamic solutions of the Goland wing model were obtained using time marching for various Mach numbers and various initial conditions. The speed of sound was set at an arbitrary value of 647 ft/s. It was found that the Goland wing' response is decaying at most Mach numbers but there is a narrow Mach number range at which the response becomes a Limit Cycle Oscillation (LCO). Figure 7(a) shows the LCO amplitude for each mode, in the form of a bifurcation plot. Up to a Mach number of 0.91 the LCO amplitude is zero, i.e. the response is decaying. At $M = 0.915$ however, the wing begins to undergo LCOs, as evidenced by the non-zero LCO amplitude in all modes. The LCO amplitude initially grows quickly, but then drops back towards zero as the Mach number is increased; the system reverts to a stable decaying behaviour after M=0.95. This type of bifurcation that causes LCOs to first appear and then disappear as a parameter is increased is usually called an 'atypical bifurcation' in aeroelasticity circles. Figure 7(a) shows that modes 1 and 2 are the main contributors to the LCO motion, with modes 3 and 4 having very low amplitudes. Therefore, the LCO observed here is an apparent bending-torsion phenomenon.

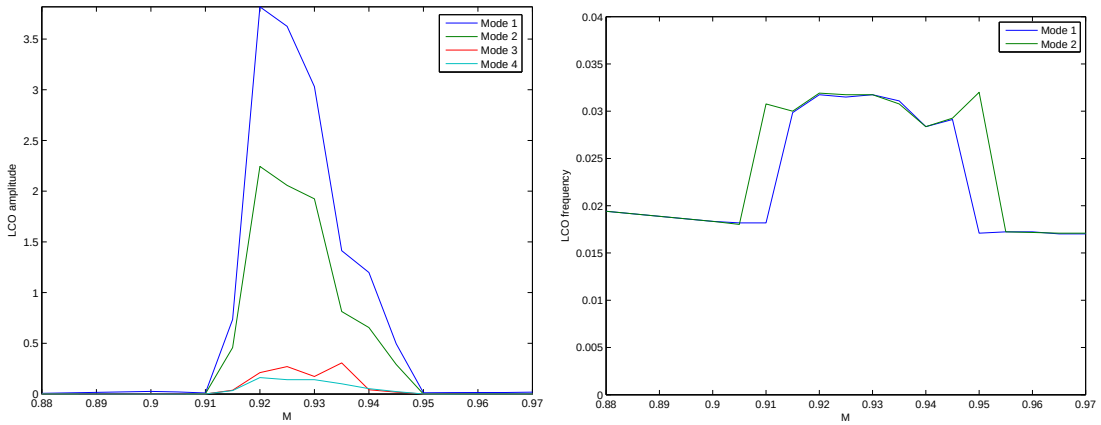

(a) LCO amplitude (b) Response frequency

Figure 7: Bifurcation behaviour of Goland wing

Figure 7(b) shows the variation of the response frequency of modes 1 and 2 with Mach number. For clarity, only the first two modes are shown. The frequency varies smoothly until the LCO Mach range is reached, at which point it jumps abruptly to a higher value. It stays at this increased value throughout the LCO region; it jumps back down to its pre-critical neighborhood at $M = 0.95$. Notice that the frequency of mode 2 jumps up at $M = 0.91$ i.e. earlier than that of mode 1; it also jumps down at $M = 0.955$, i.e. later than that of mode 1. This discrepancy suggests that nonlinear phenomena also occur outside the LCO region but their effect is not very dramatic.

With respect to the static results, the LCOs occur at the Mach number range at which the highest lift curve slopes are obtained at a zero angle of attack. Therefore, LCOs in the unsteady case are obtained at Mach numbers where the steady lift curve is most nonlinear. As mentioned in the previous section, the Mach number range at which shock waves can lie on the wing's surface at zero angle of attack is $0.885 - 0.955$. The Mach range over which LCOs can be obtained in the steady case is smaller at $0.915 - 0.945$. This fact signifies that nonlinearity does not always cause Limit Cycle Oscillations.

By making use of Short-Time Fourier Transform (STFT) and Hilber Trasform [28], the degree of nonlinearity that the shockwave presence has on the wing static response at 0° angle of attack, can be estimated. Figure 8 shows the STFT of mode 1 responses for $M = 0.9$ and $M = 0.92$ respectively. The STFT for $M = 0.9$ contains a single constant frequency throughout the duration of the response (figure 8(a)). There is no indication of nonlinearity as there are no higher harmonics and the single peak at 0.018 nondimensional frequency does not change frequency over time. At the same Mach number, the backbone curves derived via the Hilbert transform can be observed in figure 9(a). The backbones show the frequency at which the system oscillates at various vibration amplitude or damping levels. For the $M = 0.9$ case the frequency of oscillation remains constant for all amplitude and damping values, as expected from a linear system. The STFT at $M = 0.92$ shows a shift in frequency with time (figure 8(b)). Initially, there is a frequency component at 0.018 which decays and disappears momentarily. A new frequency component appears at 0.03 which carries on indefinitely. Later on the 0.018 component re-appears. The corresponding amplitude backbone curve (figure 9(b)) also displays three distinct regions. From these plots it can be concluded that a nonlinearity is present at $M = 0.92$ and this nonlinearity is stiffening in nature.

3.3 Extent of nonlinear Mach number range

In this section, the extent of the Mach range during which the aeroelastic system behaves as a nonlinear dynamic system will be quantified by means of linear system identification. It is stipulated that if the dynamic responses of the system can be used to identify a linear mathematical model with very small errors, then the original responses were obtained from a linear system.

The modal responses, $\boldsymbol{q}(t)$, of the system to initial condition excitation are used to identify a mathematical model of the form

$$\begin{pmatrix} \ddot{\boldsymbol{q}} \\ \dot{\boldsymbol{q}} \end{pmatrix} = \boldsymbol{A} \begin{pmatrix} \dot{\boldsymbol{q}} \\ \boldsymbol{q} \end{pmatrix} + \boldsymbol{b} \tag{14}$$

where $\boldsymbol{A}$ is an unknown matrix and $\boldsymbol{b}$ is an unknown vector, both of which depend on the flight condition. The modal displacements and velocities are obtained directly from the time marching solution of the CFD/CSD system. The modal accelerations are obtained by numerical differentiation of the modal velocities. A different $\boldsymbol{A}$ matrix is obtained at each test Mach

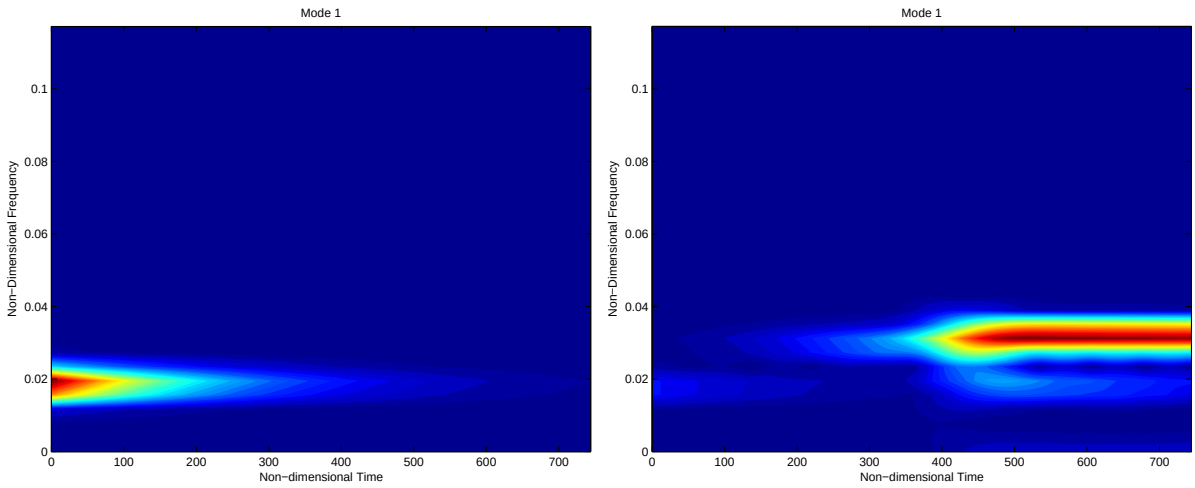

(a) $M = 0.90$ (b) $M = 0.92$

Figure 8: Short-Time Fourier Transform

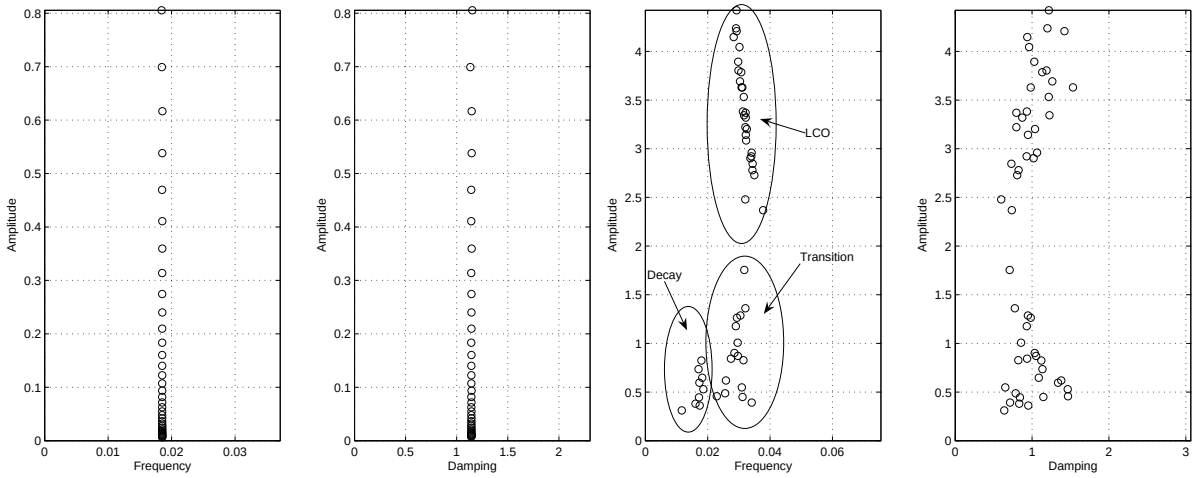

(a) $M = 0.90$ (b) $M = 0.92$

Figure 9: Hilber Trasform

number.

The modal responses are obtained as discrete realisations at N time instances, denoted by $\boldsymbol{q}_k$ for $k = 1, \ldots, N$. Equation 14 is written as

$$\begin{pmatrix} \ddot{\boldsymbol{q}}_1^T & \dot{\boldsymbol{q}}_1^T \\ \vdots & \vdots \\ \ddot{\boldsymbol{q}}_N^T & \dot{\boldsymbol{q}}_N^T \end{pmatrix} = \begin{pmatrix} \dot{\boldsymbol{q}}_1^T & \boldsymbol{q}_1^T \\ \vdots & \vdots \\ \dot{\boldsymbol{q}}_N^T & \boldsymbol{q}_N^T \end{pmatrix} \boldsymbol{A}^T + \begin{pmatrix} \boldsymbol{b}^T \\ \vdots \\ \boldsymbol{b}^T \end{pmatrix} \tag{15}$$

where the superscript T denotes the matrix or vector transpose, and is solved in a least squares sense for $\boldsymbol{A}$ and $\boldsymbol{b}$. This system identification procedure gives rise to a mathematical model of the CFD/CSD system of the form

$$\begin{pmatrix} \ddot{\boldsymbol{x}} \\ \dot{\boldsymbol{x}} \end{pmatrix} = \boldsymbol{A} \begin{pmatrix} \dot{\boldsymbol{x}} \\ \boldsymbol{x} \end{pmatrix} + \boldsymbol{b} \tag{16}$$

where $\boldsymbol{x}(t)$ are the displacements of the identified model. Equations 16 can be integrated numerically in time using a Runge-Kutta scheme or can be solved analytically. The latter approach is used here; the solution, $x(t)$, is obtained from

$$\boldsymbol{z} = \bar{\boldsymbol{K}}^{-1}\boldsymbol{b} + \sum_{i=1}^{L} a_i \boldsymbol{v}_i \exp \lambda_i t \tag{17}$$

where L is the number of modes (in this case $L = 4$), $\boldsymbol{z} = [\dot{\boldsymbol{x}}^T \quad \boldsymbol{x}^T]^T$, $\boldsymbol{v}_i$ is the ith eigenvector of matrix $\boldsymbol{A}$, λ_i is the ith eigenvalue of matrix $\boldsymbol{A}$ and a_i is the ith element of vector

$$\boldsymbol{a} = \boldsymbol{V}^{-1}\left(\boldsymbol{z}(0) + \begin{pmatrix} \boldsymbol{0} \\ \bar{\boldsymbol{K}}^{-1}\boldsymbol{b} \end{pmatrix}\right)$$

matrix $\boldsymbol{V}$ being the matrix whose columns are the eigenvectors $\boldsymbol{v}_i$. The matrix $\bar{\boldsymbol{K}}$ is obtained by splitting matrix $\boldsymbol{A}$ into

$$\boldsymbol{A} = \begin{pmatrix} \bar{\boldsymbol{C}} & \bar{\boldsymbol{K}} \\ \boldsymbol{I} & \boldsymbol{0} \end{pmatrix}$$

A model error measure, ε can be defined as

$$\varepsilon = 100\frac{\text{trace}[(\boldsymbol{X} - \boldsymbol{Q})(\boldsymbol{X} - \boldsymbol{Q})^T]}{\text{trace}[\boldsymbol{X}\boldsymbol{X}^T]} \tag{18}$$

where $\boldsymbol{Q}$ is the matrix whose columns are the modal displacements $\boldsymbol{q}_k$ for all N time instances and $\boldsymbol{X}$ is the matrix whose columns are the identified model displacements at the same time instances, $\boldsymbol{x}_k$. The function trace denotes the sum of the diagonal elements of a square matrix. A different value of ε is obtained at each Mach number.

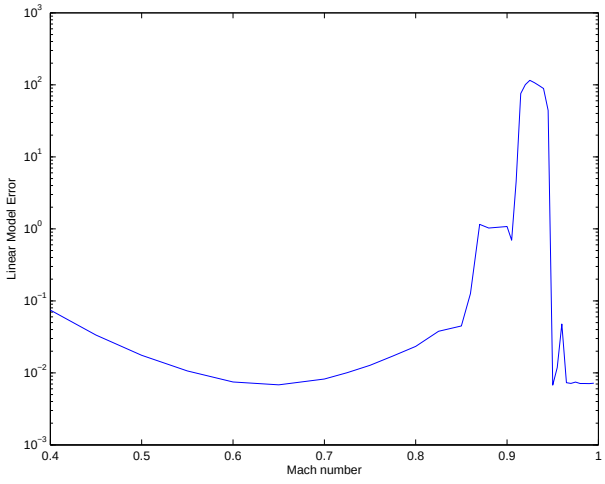

Figure 10: Linear model error for a range of Mach numbers

The responses of the CFD/CSD system were calculated using time marching at Mach numbers from 0.4 to 0.995 and curve-fitted by the linear model of equation 14. The resulting error is plotted in figure 10. It can be seen that for Mach numbers up to 0.88 the error is of the order

of 0.1%. However, in the region $M = 0.88$ and $M = 0.95$ the error is of much higher order, initially 1% and during the subsequent LCOs up to 100%. At Mach numbers higher than 0.95 the error drops to below 0.1% again.

It should be noted that the model error is never zero because the modal accelerations were obtained using numerical differentiation of the modal velocities, not directly from the CFD/CSD solution. Nevertheless, figure 10 clearly shows that the Goland wing is essentially a linear system outside a specific region Mach range of 0.88-0.95. This region also happens to be the region in which static solutions of the Goland wing predict that shock waves can exist on the surface of the wing at zero angle of attack. It can be extrapolated that the existence of these shock waves is the principal source of nonlinearity in the system.

3.4 LCO characterization

The modal displacements over a single averaged LCO period can be curve-fitted using a Fourier series to obtain an estimate of the position and order of the nonlinearity. The coefficients of the Fourier series can be obtained directly from the Fast Fourier Transform of the modal displacements. On the basis of these results a nonlinear system identification procedure was performed on the modal displacements and velocities from one period of the LCO. According to the static analysis presented earlier, the nonlinearity of the system is not affected by bending motion but clearly depends on torsional motion. Therefore, the nonlinear functions in the system cannot depend on mode 1 and should depend mostly on mode 2. Modes 3 and 4 also feature a certain amount of torsion so they may also affect the nonlinearity.

For the purposes of the present system identification procedure, nonlinear coupling between modes was ignored and only cubic polynomial basis functions were used. The terms considered were z_2^3, z_3^3, z_4^3, z_6^3, z_7^3 and z_8^3. The importance of these terms was estimated using a backwards elimination scheme. The final nonlinear model was of the form

$$\dot{\boldsymbol{z}} = \boldsymbol{A}z + \boldsymbol{C}\begin{pmatrix} z_3 \\ z_6 \end{pmatrix}^3 \tag{19}$$

where $\boldsymbol{A}$ and $\boldsymbol{C}$ are unknown coefficients.

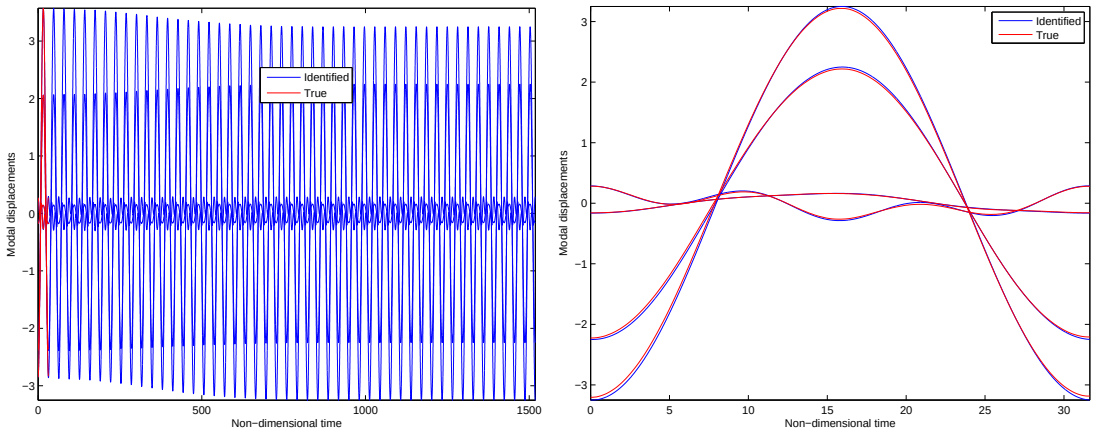

(a) Response over 48 periods (b) Response over last period only

Figure 11: Comparison of true and identified modal displacements

The complete identified model was then integrated using a first order finite difference scheme to

obtain the identified model's responses to initial condition excitation on the LCO. The comparison between the true and identified modal displacements can be seen in figure 11. Figure 11(a) shows the response of the identified model over 48 periods. It can be seen that the shape of the limit cycle is preserved but its centrepoint changes, moving towards zero. This effect is due to the fact that the model chosen for the identification did not contain a constant term. Figure 11(b) shows the identified LCO over the last period of the simulation, compared to the true LCO re-centred around 0. It can be seen that the two lines are very similar.

The identification presented here should not be seen as a complete nonlinear system identification. It should be viewed more as a means of characterising the LCO. There exists only a narrow range of initial conditions that will allow the identified model to converge on the true LCO. Outside this range the model fails. However, the analysis demonstrates that the nonlinear responses of the full CFD/CSD system can be described by a relatively low order model which is valid in the neighbourhood of the limit cycle oscillations.

4 CONCLUSIONS

This paper attempts to describe and characterize the nonlinearity of a coupled CFD/CSD solution of a simple rectangular wing with store, known as the Goland wing. Static aerodynamic solutions are used to demonstrate that the nonlinearity only occurs in a narrow range of Mach numbers at which shock waves can exist on the surface of the wing, while present a fully linear behaviour outside this region, even in the transonic regime. Dynamic solutions of the wing showed that nonlinear effects can be observed in exactly the Mach range predicted by the static results. The nonlinearity affects primarily torsional vibrations.

Within the nonlinear Mach range there exists a smaller range where Limit Cycle Oscillations can occur. The LCOs were investigated by means of phase portraits, Fourier analysis and nonlinear system identification. It is shown that the wing undergoing LCO motion can be approximated by a very small order model using four modes and polynomial nonlinearity. While this model is not a complete description of the true system, it serves to demonstrate that the important dynamics of the full coupled CFD/CSD model can be described by simple, low order models.

The nonlinearity of the full CFD/CSD aeroelastic system depends on flight condition and there are two main flight condition, one of which causes the system to be linear and one to be nonlinear. Therefore, it is shown that two different types of Reduced Order Model can be used to describe the system, a linear modal model in the linear Mach number range and a nonlinear model in the Mach range where LCOs can occur.

ACKNOWLEDGEMENTS

The authors would like to thank the Engineering and Physical Sciences Research Council of the United Kingdom.

5 REFERENCES

[1] S.A. Dunn, P.A. Farrell, P.J. Budd, P.B. Arms, C.A. Hardie, and C.J. Rendo. F/A-18A flight flutter testing-limit cycle oscillation or flutter? In *International Forum on Aeroelasticity and Structural Dynamics*, Madrid, Spain, June 2001.

[2] S.J. Price, H. Alighambari, and B.H.K. Lee. The aeroelastic response of a two-dimensional airfoil with bilinear and cubic structural nonlinearities. *Journal of Fluids and Structures*, 9:175–193, 1995.

[3] B.H.K. Lee, S.J. Price, and Y.S. Wong. Nonlinear aeroelastic analysis of airfoils: bifurcation and chaos. *Progress in Aerospace Sciences*, 35:205–334, 1999.

[4] M.D. Conner, D.M. Tang, E.H. Dowell, and L.N. Virgin. Nonlinear behavior of a typical airfoil section with control surface freeplay: a numerical and experimental study. *Journal of Fluids and Structures*, 11:89–109, 1997.

[5] G.A. Vio and J.E. Cooper. Limit cycle oscillation prediction for aeroelastic systems with discrete bilinear stiffness. *International Journal of Applied Mathematics and Mechanics*, 3:100–119, 2005.

[6] L. Liu and E.H. Dowell. Harmonic balance approach for an airfoil with a freeplay control surface. *AIAA Journal*, 43(4):802–815, 2005.

[7] G. Dimitriadis, G. A. Vio, and J. E. Cooper. Application of higher-order harmonic balance to non-linear aeroelastic systems. In *Proceedings of the* 47^{th} *AIAA/ASME/ASCE/AHS/ASC Structures, Structural Dynamics and Materials Conference*, Newport, Rhode Island, May 2006.

[8] G. A. Vio, G. Dimitriadis, and J. E. Cooper. Bifurcation analysis and limit cycle oscillation amplitude prediction methods applied to the aeroelastic galloping problem. *To appear in the Journal of Fluids and Structures*, 2007.

[9] G.A. Vio, G. Dimitriadis, and J.E. Cooper. On the solution of the aeroelastic galloping problem. In *International Conference on Noise and Vibration Engineering, ISMA 2004*, Leuven, Belgium, September 2004.

[10] E. H. Dowell, K. C. Hall, J. P. Thomas, R. Florea, B. I. Epureanu, and J. Heeg. Reduced order models in unsteady aerodynamics. *Engineering Mechanics*, 6(4-5):229–252, 1999.

[11] W.A. Silva, T.W. Strganac, and M.R. Hajj. Higher-order spectral analysis of a nonlinear pitch and plunge apparatus. In *Structures, Structural Dynamics and Materials Conference*, Austin, Texas, USA, April 2005.

[12] A. L. Gaitonde and D. P. Jones. Reduced order state-space models from the pulse responses of a linearized CFD scheme. *International Journal for Numerical Methods in Fluids*, 42(6):581–606, 2004.

[13] W. Silva. Identification of nonlinear aeroelastic systems based on the Volterra theory: Progress and opportunities. *Nonlinear Dynamics*, 39(1-2):25–62, 2005.

[14] D. J. Lucia, P. S. Beran, and W. A. Silva. Aeroelastic system development using proper orthogonal decomposition and Volterra theory. *Journal of Aircraft*, 42(5):509–518, 2005.

[15] K. Willcox and J. Peraire. Balanced model reduction via the proper orthogonal decomposition. *AIAA Journal*, 40(11):2323–2330, 2002.

[16] S. A. Mortara, J. Slater, and P. Beran. Analysis of nonlinear aeroelastic panel response using proper orthogonal decomposition. *Journal of Vibration and Acoustics*, 126(3):416–421, 2004.

[17] G. A. Vio, G. Dimitriadis, J. E. Cooper, K. J. Badcock, M.A. Woodgate, and A. M. Rampurawala. Aeroelastic system identification using transonic CFD data for a wing/store configuration. *Aerospace Science and Technology*, 11(2-3):146–154, 2007.

[18] K. J. Badcock, B.E. Richards, and M.A. Woodgate. Elements of computational fluid dynamics on block structured grids using implicit solvers. *Progress in Aerospace Sciences*, 36:351–392, 2000.

[19] S. Osher and S. Chakravarthy. Upwind schemes and boundary conditions with applications to Euler equations in general geometries. *Journal of Computational Physics*, 50:447–481, 1983.

[20] B. Van Leer. Towards the ultimate conservative conservative difference scheme II: Monotonicity and conservation combined in a second order scheme. *Journal Computational Physics*, 14:361–374, 1974.

[21] F. Cantaritti, L. Dubuc, B. Gribben, M. Woodgate, K. Badcock, and B. Richards. Approximate Jacobian for the solution of the Euler and Navier-Stokes equations. Aerospace engineering report, University of Glasgow, 1997.

[22] A. Jameson. Time dependant calculations using multigrid, with applications to unsteady flows past airfoils and wings. Technical Report 91-1596, AIAA, 1991.

[23] G.S.L. Goura, K.J. Badcock, M.A. Woodgate, and B.E. Richards. Extrapolation effects on coupled CFD-CSD simulations. *AIAA Journal*, 41(2):312–314, 2003.

[24] W.J. Gordon and C.A. Hall. Construction of curvilinear coordinate systems and applications to mesh generation. *International Journal of Numerical Methods in Engineering*, 7:461–477, 1973.

[25] G.S.L. Goura, K.J. Badcock, M.A. Woodgate, and B.E. Richards. Implicit method for the time marching analysis of flutter. *Aeronautical Journal*, 105(1046):119–214, 2001.

[26] M. Goland. The flutter of a uniform cantilever wing. *Journal of Applied Mechanics*, 12(4):197–208, 1945.

[27] P.S. Beran, N.S. Khot, F.E. Eastep, R.D. Snyder, and J.V. Zweber. Numerical analysis of store-induced limit-cycle oscillation. *Journal of Aircraft*, 41(6):1315–1326, 2004.

[28] G. A. Vio, G. Dimitriadis, J. E. Cooper, K. Badcock, M. Woodgate, and A. Rampurawala. Aeroelastic system identification using transonic CFD data for a 3D wing. In *Recent Advances In Structural Dynamics*, Southampton, UK, July 2006.